Editors' Suggestion | Featured in Physics

Enrichment of Scavenged Particles in Jet Drops Determined by Bubble Size and Particle Position

Lena Dubitsky,* Oliver McRae,* and James C. Bird†
Department of Mechanical Engineering, Boston University, Boston, Massachusetts 02215, USA

(Received 8 June 2022; revised 4 November 2022; accepted 6 January 2023; published 3 February 2023)

When small bubbles rupture in a contaminated water source, the resulting liquid jet breaks up into droplets that can aerosolize solid particulates such as bacteria, viruses, and microplastics. Particles collected on the bubble surface have the potential to become highly concentrated in the jet drops, dramatically increasing their impact. It has been assumed that only particles small enough to fit within a thin microlayer surrounding the bubble can be transported into its influential top jet drop. Yet here, we demonstrate that not only can larger particles be transported into this jet drop, but also that these particles can exceed previous enrichment measurements. Through experiments and simulations, we identify the prerupture location of the liquid that develops into the top jet drop and model how interfacial rearrangement combines with the bubble size, particle size, and the angular distribution of particles on the bubble surface to set the particle enrichment.

DOI: 10.1103/PhysRevLett.130.054001

Once bubbles rise to the surface of a pool of water, they burst and can create jet drops from the erupting jet and film drops from the retracting bubble film. These drops are critical to health [1–5] and the environment [6–9], as they can carry bacteria [10], viruses [11], and pollutants such as microplastics [12,13] into the air. Because of the importance of droplets and their cargo, much work has been devoted to understanding the number and size of droplets emitted by a bursting bubble [14–21]. However, predicting the number of particles in a drop requires more than knowing the bulk particle concentration and the drop size: particles can accumulate on the surface of a rising bubble and transfer into the droplets. This mechanism can dramatically increase the droplet particle concentration [22,23].

When will a particle on a bubble end up in its top jet drop? This unresolved question is essential to understanding and predicting the extent of jet drop enrichment. Pioneering experiments concluded that the liquid in the top jet drop comes exclusively from a thin liquid microlayer surrounding the bubble [24]. When there are particles scavenged on the bubble surface, it is expected that these particles passively advect with the fluid. All particles small enough to fit within the inner-most microlayer are thus assumed to collect into the top jet drop; whereas those that extend beyond this microlayer have been proposed to end up elsewhere [25]. These expectations are consistent with foundational observations by Blanchard and Syzdek [22] that jet drops of radius $r_d = 60$ μm had a higher average bacterial concentration than either smaller or larger jet drops. Enrichment peaks have been reported by other researchers [26–28]; however, their existence has been questioned as similar experiments did not observe a peak [29]. The existence of enrichment peaks has significant implications for the transport of particles larger than the microlayer thickness, as it could strongly enhance or deplete viruses in small drops or microplastics in larger ones. However, past studies have used particles of radius $r_p \approx 0.5$ μm, making it difficult to generalize to different particle and microlayer sizes. Furthermore, discerning the precise dependence of enrichment on particle size is challenging due to the inherent variability in these systems. Even within carefully controlled experiments, enrichment under identical conditions is highly variable [30]. In this Letter, we demonstrate that particles significantly larger than the microlayer thickness can be transported into the top jet drop and still exhibit an enrichment peak (Fig. 1). This observation motivates a transport model that depends on the relative sizes of the particle, bubble, and jet drop, as well as the angular location of particles on the bubble just before bursting. Stochasticity in this last factor may underlie the high variability of jet drop enrichment.

Our experimental setup is shown in Fig. 1(a). Polystyrene beads of either radius $r_p = 7.5$ μm or 15 μm and density $\rho_p = 1050$ kg/m^3 are suspended in water at a concentration of $C = 10^5$ and 10^4 particles/mL, respectively. A needle releases an air bubble at a depth $H = 5.5$ cm and the bubble scavenges particles as it rises through a container filled with 75 mL of solution. We vary the bubble radius R_b between 250 and 730 μm, such that the bubbles are small enough to limit gravitational effects on bubble shape and jet drop size and large enough that we are able to appropriately resolve the top drop with high-speed imaging [20,31]. Upon reaching the free surface, the bubble ruptures and the air cavity collapses, resulting in jet

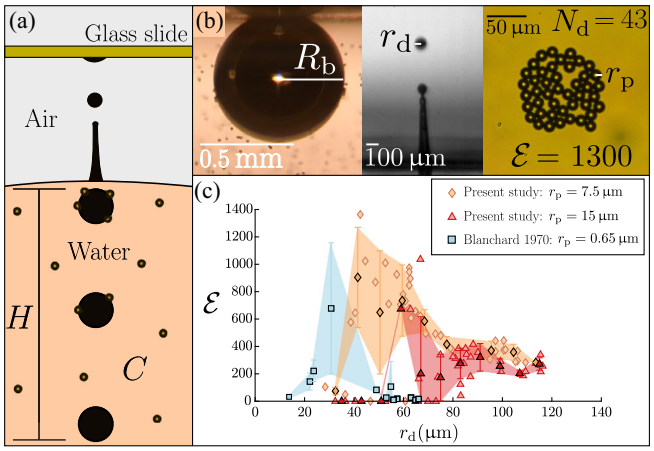

FIG. 1. Polystyrene microparticles (radius $r_p = 7.5$ and 15 μm) exhibit enrichment peaks in jet drops. (a) Schematic of experiments: bubbles rise a height H through a solution of uniform particle size at concentration C particles/mL. The bubble scavenges particles as it rises and the top jet drop is collected. (b) A bubble with radius $R_b = 350$ μm creates a jet drop with radius $r_d = 43$ μm that contains $N_d = 43$ particles, corresponding to an enrichment factor $\mathcal{E} = 1300$. (c) Measured enrichment [Eq. (1)] for both particle sizes and historical data from Blanchard and Syzdek [22].

droplets. Consistent with past studies, we collect the top jet drop on a glass slide to count the number of particles (Fig. S1) [22,28,29].

Because we directly measure and link each bubble, jet drop, and particle count, we can precisely determine the enrichment factor. For example, Fig. 1(b) shows a $R_b = 350$ μm bubble with $r_p = 7.5$ μm particles on its surface. High-speed imaging captures the resulting $r_d = 43$ μm jet drop. If there were no enrichment mechanism, there is only a 3% chance that the volume would contain a single particle. In reality, the drop contains $N_d = 43$ particles, an increase by a factor of 1300. This enrichment occurs because the bubble is surrounded by a concentrated number of particles N_b immediately before rupture and a significant fraction of them, E_t, transfer into the top droplet. Therefore the enrichment factor $\mathcal{E}$, which is the ratio of jet drop to solution particle concentration, can be expressed as

$$\mathcal{E} = \frac{N_d}{\frac{4}{3}\pi r_d^3 C} = \frac{N_b}{\frac{4}{3}\pi r_d^3 C} E_t. \tag{1}$$

We observe enrichment factors from zero to over 1000 over a range of jet drop sizes for the two particle sizes tested [Fig. 1(c)]. The larger symbols with error bars show the enrichment mean and standard deviation for sets of data with different jet drop sizes, with shading connecting these error bars as a guide for the eye. Both the average enrichment factor and its standard deviation rise and then decline as the jet drop size decreases, demonstrating the existence of enrichment peaks for these relatively large particle sizes.

To incorporate the physics of bubble scavenging into the enrichment factor, we approximate the number of particles on the bubble surface immediately before rupture as $N_b = E_c E_a \pi R_b^2 HC$, where E_c is the collision efficiency, E_a is the attachment efficiency, H is the bubble rise height, and C is the particle concentration in the fluid [32,33]. This general expression can be simplified for our particular experiments by noting that the attachment efficiency $E_a \approx 1$ and that the particle sizes are consistent with those scavenged through interception (see Supplemental Material [34]). Following an approach used to model enrichment in film drops [23], we consider a simple potential flow interception model, $E_c = 3(r_p/R_b)$, developed by Sutherland [41]. Thus enrichment is approximated as

$$\mathcal{E} \approx \frac{3H}{4R_b}\frac{r_p}{\ell} E_t, \tag{2}$$

where $\ell \equiv r_d^3/(3R_b^2)$ is the microlayer thickness used conceptually in previous models [25,28,29]. Specifically, ℓ is the thickness of a uniform film surrounding the bubble that has the same volume as the top jet drop.

All previous enrichment models assume that every particle on the bubble surface transfers to the top jet drop ($E_t = 1$) if the particle fully fits inside of the microlayer ($2r_p < \ell$) [25,28,29]. Therefore, as the bubble size gets smaller, the enrichment is expected to increase [Eq. (2)]. The enrichment peaks previously observed were rationalized through the exclusion of particles larger than the microlayer thickness ($E_t = 0$), creating a peak enrichment at $r_p \sim \ell$. However, because $r_p \gg \ell$ for all of our experiments, this theory predicts that none of the top jet drops should have contained particles, in contrast to our results (Fig. 1). Recently, it has been suggested that the transfer efficiency need not go to zero for particles larger than ℓ, but rather decays as $E_t = \ell/(2r_p)$ [29]. Consequently this expression, when substituted into Eq. (2), predicts an enrichment that increases monotonically with decreasing bubble radius and is therefore inconsistent with the enrichment peaks observed in our experiments. Furthermore, this alternative criterion underestimates the extent of the large particle enrichment by an order of magnitude. Therefore it is natural to ask whether the mechanism to transfer particles from the bubble surface to the jet drop is set by factors other than the microlayer length scale ℓ.

Here, we propose an alternate particle filtering mechanism based on the thickness of a microlayer that has been compressed during the bubble rupture process. We note that particles are swept to the base of the bubble as it ruptures, and as they do so we conjecture that the interfacial bubble area on which they are attached compresses from $dA_0 \sim R_b^2$ to $dA_c \sim r_d^2$. Thus particles would be contained within fluid destined for the top jet provided that they were smaller than the compressed film thickness $h_c \sim \ell(dA_0/dA_c) \sim \ell(R_b^2/r_d^2) = r_d/3$.

To develop and quantify the proposed transfer efficiency model, we carry out numerical simulations (Fig. 2). We simulate the bubble bursting and jetting process by solving the two-phase incompressible Navier-Stokes equations using the volume-of-fluid solver Gerris [31,42–46]. A $R_b = 350$ μm air bubble in water is initialized with a small hole in its cap (Fig. S2). As time progresses, capillary waves travel down the bubble cavity, meet at the base of the bubble, and create a fluid jet that breaks up into jet drops [Fig. 2(a)]. A key assumption in past models is that all the fluid within a uniform microlayer ℓ ends up in the top jet drop [25,28,29], yet Lagrangian tracking shows that many fluid parcels that were initially in the microlayer ℓ are stretched throughout the fluid jet at the time of drop pinch-off [left side of Fig. 2(a)]. Here, darker marker colors signify larger parcel volumes due to the axisymmetric geometry. By mass conservation, the presence of liquid outside of the top jet that originated within ℓ implies that some liquid within the jet drop originated beyond ℓ. Indeed, this conclusion is consistent with a non-uniform microlayer [Fig. 2(a)(vi), right], which was originally envisioned for this skimming process yet never quantified [24]. To determine how the volume of the fluid in the top jet was originally distributed around the bubble, we track the liquid parcels backward in time [right side of Fig. 2(a)]. These volumes are then converted to a microlayer thickness h_0 at each angle (θ) (Fig. S3). The computed microlayer $h_0(\theta)$ has a nontrivial profile with three regions that are thinner than ℓ [Fig. 2(b)]. These depletion zones align with the three streams of forward-tracked liquid that were excluded from the jet drop [Fig. 2(a), left].

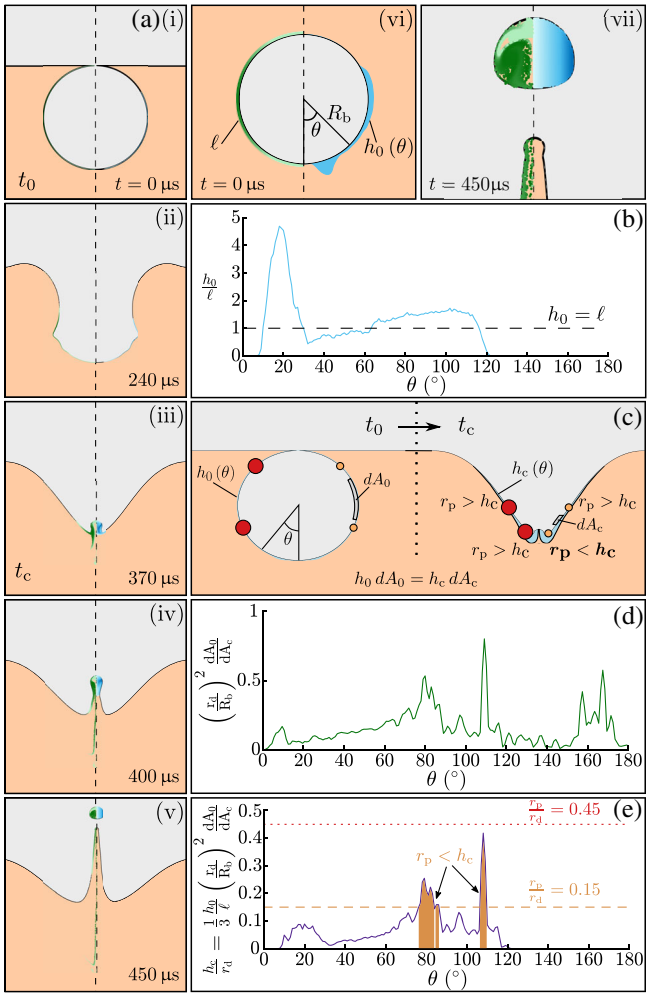

FIG. 2. The modified filtration mechanism is developed numerically for a $R_b = 350$ μm bubble. (a) Bubble rupture creates a fluid jet at time t_c [(i)–(iii)], which then forms a jet drop r_d [(iv)–(v)]. Lagrangian particle tracking reveals that not all of the fluid in the microlayer ℓ [(vi), left] ends up in the top drop [(vii), left]. Reverse Lagrangian tracking finds that the fluid in the top drop [(vii), right] comes from a layer whose thickness h_0 varies with angle θ at $t = 0$ [(vi), right], where the thickness has been exaggerated for clarity. (b) Plot comparing h_0 to ℓ highlights a strong dependence on the initial angle θ. (c) Schematic illustrating the proposed particle exclusion mechanism. The bubble interface on which particles are attached compresses from a surface area dA_0 to dA_c, which locally thickens h_0 to h_c and provides an exclusion criterion when $r_p > h_c$. (d) Local compression dA_0/dA_c normalized by $(R_b/r_d)^2$ approaches one. (e) The compressed thickness h_c varies with angle and reaches nearly half the jet drop size. A particle with $r_p = 0.45 r_d$ (red dotted line) would be excluded from the top jet drop; whereas a smaller particle $r_p = 0.15 r_d$ (yellow dashed line) would be included only at certain angles on the bubble, following the proposed exclusion criteria.

Instead of considering a particle exclusion criteria based on the microlayer thickness $h_0(\theta)$ at time t_0, we consider the thickness of the compressed film $h_c(\theta)$ at the onset of jetting t_c [Fig. 2(c)]. By measuring the changing separation and radial position of nearby points on the bubble surface during the forward Lagrangian tracking, we can compute the local interfacial compression (Fig. S4). At time t_c, the local area compression dA_c/dA_0 approaches $(R_b/r_d)^2$, with the precise value depending on material coordinate θ [Fig. 2(d)]. Because the volume of each interfacial element is conserved, $h_c = h_0 dA_0/dA_c$. Therefore, h_c/r_d can be directly related to the product of the functions illustrated in Figs. 2(b) and 2(d), with the values h_c ranging from 0 to $0.43 r_d$ [Fig. 2(e)]. For particles within this size range, whether or not the particle extends beyond h_c—our proposed exclusion criterion—depends on the particle's initial angular position.

To extend the model to other bubble sizes, we repeat the steps outlined in Fig. 2 for a range of Ohnesorge numbers $\mathrm{Oh} \equiv \mu/\sqrt{\rho\gamma R_b}$, where μ, ρ, and γ are the liquid viscosity, density, and surface tension, respectively (Fig. 3). Numerous studies have investigated the relationship between r_d and R_b, finding that it decreases as Ohnesorge number increases up to $\mathrm{Oh} \lesssim 0.03$, corresponding to a $R_b = 14$ μm bubble in water [20]. We limit our numerical simulations within this Oh range and find that

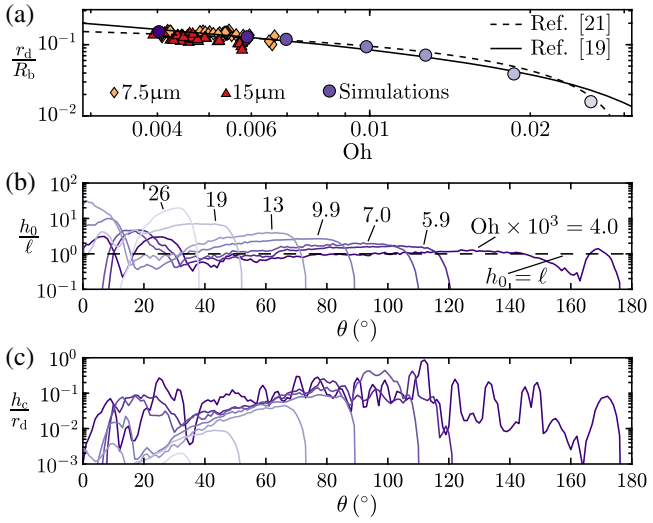

FIG. 3. Extending numerics to additional bubble sizes via an Ohnesorge number, Oh. (a) Experimental and numerical values of r_d/R_b vary with $\mathrm{Oh} \equiv \mu/\sqrt{\rho\gamma R_b}$, where μ, ρ, and γ are the liquid viscosity, density, and surface tension, respectively. Values are consistent with existing theory (solid [19] and dashed lines [21]). (b) The thickness h_0/ℓ depends on both angle θ and Oh. (c) Plots of h_c/r_d similarly show that for higher Oh the top jet drop fluid is drawn from an increasingly smaller portion of the bubble.

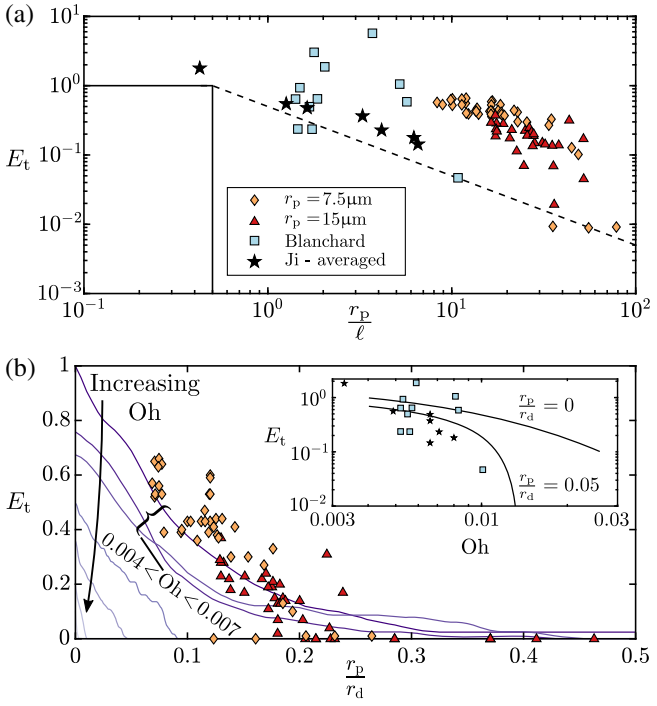

FIG. 4. Particle transfer efficiencies E_t between experiments and models are compared. (a) Experimental transfer efficiency is approximated as $E_t = (4R_b/3H)(\ell/r_p)\mathcal{E}$ for the present study as well as for Refs. [22] and [29]. Previous enrichment models have relied on the microlayer thickness ℓ and underpredict values of E_t (solid [25] and dashed lines [29]). (b) The transfer efficiency modeled by Eq. (3) depends on both r_p/r_d and Oh (solid lines). These values can be plotted with contours of constant Oh (main) or contours of constant r_p/r_d (inset) from numerics. In all experiments, both r_p/r_d and Oh change as the bubble size varies. The modeled E_t values are consistent with our experimental results for which $0.004 < \mathrm{Oh} < 0.007$.

experimental and numerical r_d/R_b values agree well with analytical expressions [19,21] [Fig. 3(a)]. The values for h_0/ℓ and h_c/r_d are computed for the range of Oh, showing a strong angular dependence of the initial and compressed fluid layers that varies with Oh [Figs. 3(b) and 3(c)]. For example, our experimental bubble sizes are within $0.004 < \mathrm{Oh} < 0.007$. A $R_b = 750$ μm bubble ($\mathrm{Oh} = 0.004$) has a top drop compressed fluid layer thickness h_c that extends nearly to 180°, while a $R_b = 250$ μm bubble ($\mathrm{Oh} = 0.007$) has a fluid layer that stops at ≈110°. Meanwhile, the smallest bubble simulated ($R_b = 18$ μm, $\mathrm{Oh} = 0.026$) has a compressed fluid layer h_c that only extends to 40° on the bubble [Fig. 3(c)], suggesting that particles attached on the upper three-quarters of the bubble surface would be excluded from the top jet drop, regardless of size.

We model the transfer efficiency $E_t(r_p/r_d, \mathrm{Oh})$ by combining the numerical results [Fig. 3(c)] with our proposed particle exclusion mechanism:

$$E_t = \int_0^\pi \widetilde{E}_t(\theta)\frac{\sin\theta}{2}d\theta, \qquad \widetilde{E}_t = \begin{cases} 1, & r_p < h_c(\theta, \mathrm{Oh}) \\ 0, & r_p > h_c(\theta, \mathrm{Oh}) \end{cases}. \tag{3}$$

A particle at angle θ is transferred to the top drop ($\tilde{E}_t = 1$) if its size r_p is less than the local compressed layer thickness h_c. The total E_t is found by spatially averaging the discrete $\tilde{E}_t$ values over the entire surface area of the bubble. Note that if $h_c = \ell/2$ everywhere, E_t would reduce to Blanchard's criterion [25] [Fig. 4(a)]. However, our analysis illustrates that the thickness h_c varies significantly with Oh and the angle θ.

To compare the various models with present and past experimental data, we convert measured enrichment to transfer efficiencies by rearranging Eq. (2) and plot against r_p/ℓ [Fig. 4(a)]. The solid [25] and dotted [29] lines show previous transfer efficiency expressions based on the microlayer thickness ℓ, which underestimate our experimental E_t by an order of magnitude. In contrast, our model shows good agreement with the experimental data while providing an underlying mechanism for fractional E_t values [Fig. 4(b)]. Here, E_t is plotted on a linear scale, as our model predicts that E_t will become zero when r_p/r_d exceeds a critical value. Our model also predicts that E_t will decrease when Oh increases, illustrated by constant Oh contours [Fig. 4(b)]. For our range of experiments, $0.004 < \mathrm{Oh} < 0.007$, the curves slightly underestimate the measured values. A nonuniform particle distribution

observed in our experiments may contribute to this discrepancy as it is not accounted for in our spatial averaging (Fig. S5). For particles much smaller than r_d, such as those in past studies, our model suggests that the Oh will play an important role in setting the transfer efficiency. Indeed, even in the limit of $r_p = 0$, E_t decreases with increasing Oh [Fig. 4(b) inset].

We can approximate the transfer efficiency as $E_t \approx (1 + [\mathrm{Oh}/\mathrm{Oh}^*]^2)^{-1} - (1/h^*)(r_p/r_d)$, where $\mathrm{Oh}^* = 0.01$ and $h^* = 1/4$. The first term represents the fraction of the bubble surface that ends up in the top drop with Oh^* corresponding to the case where the bottom half ends up in the top drop and the top half does not. The second term takes account of the compressed thickness relative to the particle size. Here, h^* corresponds to the larger values of h_c/r_d in Fig. 3(c), which are approximately $1/4$ for $\mathrm{Oh} < \mathrm{Oh}^*$ and then decrease as Oh increases. This model suggests that particles may be selectively aerosolized based on r_p, which we confirm (Fig. S6).

Our findings suggest that whether a particle ends up in the top jet drop depends on the bubble Ohnesorge number, the ratio of the particle size to the jet drop size, and the particle angular position on the bubble. Our results contradict past enrichment theory in two crucial ways. For larger particles approaching the jet drop size, such as microplastics, we demonstrate that a significant fraction are still transported into the top jet drop, provided the Ohnesorge number is sufficiently small. Whereas for smaller particles, such as viruses and bacteria, our model predicts that a decreasing fraction will be transported into the top jet drop as bubble size decreases, even when they are smaller than the uniform microlayer thickness ℓ. We anticipate our model can be extended to nonuniform particle distributions on the bubble, which could significantly enhance or deplete the enrichment. Furthermore, the inherent variability seen in past enrichment studies follows naturally from the angular dependence in our model. Because the transfer efficiency is composed of binary outcomes as a function of angle, the enrichment variability would peak when the transfer efficiency is around 0.5, analogous to the variance in a binomial distribution. Collectively, these findings are a key step toward advancing the modeling of jet drop enrichment, which is central to the physics of air-sea exchange and climate science, environmental pollutant transport, and pathogen transmission.

We thank G. B. Deane and M. D. Stokes for helpful discussions. This work was supported by the National Science Foundation under Grant No. 2114489 and the National Science Foundation Graduate Research Fellowship Program under Grant No. DGE-1840990.

*These authors contributed equally to this work.
†Corresponding author.
jbird@bu.edu

[1] D. Johnson, R. Lynch, C. Marshall, K. Mead, and D. Hirst, Aerosol generation by modern flush toilets, Aerosol Sci. Technol. **47**, 1047 (2013).
[2] G. M. Wilson, V. B. Jackson, L. D. Boyken, M. L. Schweizer, D. J. Diekema, C. A. Petersen, P. J. Breheny, M. W. Nonnenmann, E. N. Perencevich, C. P. E. Program *et al.*, Bioaerosols generated from toilet flushing in rooms of patients with clostridioides difficile infection, Infect. Control Hosp. Epidemiol. **41**, 517 (2020).
[3] J. H. Schreck, M. J. Lashaki, J. Hashemi, M. Dhanak, and S. Verma, Aerosol generation in public restrooms, Phys. Fluids **33**, 033320 (2021).
[4] D. B. Jernigan, J. Hofmann, M. S. Cetron, J. Nuorti, B. Fields, R. Benson, R. Breiman, H. Lipman, R. Carter, C. Genese *et al.*, Outbreak of Legionnaires' disease among cruise ship passengers exposed to a contaminated whirlpool spa, Lancet **347**, 494 (1996).
[5] L. T. Angenent, S. T. Kelley, A. S. Amand, N. R. Pace, and M. T. Hernandez, Molecular identification of potential pathogens in water and air of a hospital therapy pool, Proc. Natl. Acad. Sci. U.S.A. **102**, 4860 (2005).
[6] E. R. Lewis and S. E. Schwartz, *Sea Salt Aerosol Production: Mechanisms, Methods, Measurements, and Models* (American geophysical union, Washington, DC, 2004), Vol. 152.
[7] P. J. DeMott, T. C. Hill, C. S. McCluskey, K. A. Prather, D. B. Collins, R. C. Sullivan, M. J. Ruppel, R. H. Mason, V. E. Irish, T. Lee *et al.*, Sea spray aerosol as a unique source of ice nucleating particles, Proc. Natl. Acad. Sci. U.S.A. **113**, 5797 (2016).
[8] X. Wang, G. B. Deane, K. A. Moore, O. S. Ryder, M. D. Stokes, C. M. Beall, D. B. Collins, M. V. Santander, S. M. Burrows, C. M. Sultana *et al.*, The role of jet and film drops in controlling the mixing state of submicron sea spray aerosol particles, Proc. Natl. Acad. Sci. U.S.A. **114**, 6978 (2017).
[9] L. A. Ladino, G. B. Raga, H. Alvarez-Ospina, M. A. Andino-Enríquez, I. Rosas, L. Martínez, E. Salinas, J. Miranda, Z. Ramírez-Díaz, B. Figueroa *et al.*, Ice-nucleating particles in a coastal tropical site, Atmos. Chem. Phys. **19**, 6147 (2019).
[10] A. Woodcock, Note concerning human respiratory irritation associated with high concentrations of plankton and mass mortality of marine organisms, J. Mar. Res. **7**, 56 (1948), https://peabody.yale.edu/explore/publications/journal-marine-research.
[11] E. R. Baylor, V. Peters, and M. B. Baylor, Water-to-air transfer of virus, Science **197**, 763 (1977).
[12] S. Allen, D. Allen, K. Moss, G. Le Roux, V. R. Phoenix, and J. E. Sonke, Examination of the ocean as a source for atmospheric microplastics, PLoS One **15**, 1 (2020).
[13] M. Masry, S. Rossignol, B. Temime Roussel, D. Bourgogne, P. O. Bussière, B. R'mili, and P. Wong-Wah-Chung, Experimental evidence of plastic particles transfer at the water-air interface through bubble bursting, Environ. Pollut. **280**, 116949 (2021).
[14] C. Kientzler, A. B. Arons, D. C. Blanchard, and A. Woodcock, Photographic investigation of the projection of droplets by bubbles bursting at a water surface, Tellus **6**, 1 (1954).

[15] D. C. Blanchard and L. D. Syzdek, Film drop production as a function of bubble size, J. Geophys. Res. **93**, 3649 (1988).
[16] D. E. Spiel, The sizes of the jet drops produced by air bubbles bursting on sea-and fresh-water surfaces, Tellus, Ser. B **46B**, 325 (1994).
[17] H. Lhuissier and E. Villermaux, Bursting bubble aerosols, J. Fluid Mech. **696**, 5 (2012).
[18] E. Ghabache, A. Antkowiak, C. Josserand, and T. Séon, On the physics of fizziness: How bubble bursting controls droplets ejection, Phys. Fluids **26**, 121701 (2014).
[19] A. M. Gañán-Calvo, Revision of Bubble Bursting: Universal Scaling Laws of Top Jet Drop Size and Speed, Phys. Rev. Lett. **119**, 1 (2017).
[20] C. F. Brasz, C. T. Bartlett, P. L. Walls, E. G. Flynn, Y. E. Yu, and J. C. Bird, Minimum size for the top jet drop from a bursting bubble, Phys. Rev. Fluids **7**, 074001 (2018).
[21] F. J. Blanco-Rodríguez and J. M. Gordillo, On the sea spray aerosol originated from bubble bursting jets, J. Fluid Mech. **886**, 1 (2020).
[22] D. C. Blanchard and L. Syzdek, Mechanism for the water-to-air transfer and concentration of bacteria, Science **170**, 626 (1970).
[23] P. L. Walls and J. C. Bird, Enriching particles on a bubble through drainage: Measuring and modeling the concentration of microbial particles in a bubble film at rupture, Elementa **5**, 230 (2017).
[24] F. MacIntyre, Flow patterns in breaking bubbles, J. Geophys. Res. **77**, 5211 (1972).
[25] D. C. Blanchard, The ejection of drops from the sea and their enrichment with bacteria and other materials: A review, Estuaries **12**, 127 (1989).
[26] H. Bezdek and A. Carlucci, Surface concentration of marine bacteria 1, Limnol. Oceanogr. **17**, 566 (1972).
[27] T. Hejkal, P. LaRock, and J. Winchester, Water-to-air fractionation of bacteria, Appl. Environ. Microbiol. **39**, 335 (1980).
[28] M. Sakai, A. Tanaka, H. Egawa, and G. Sugihara, Enrichment of suspended particles in top jet drops from bursting bubbles, J. Colloid Interface Sci. **125**, 428 (1988).
[29] B. Ji, A. Singh, and J. Feng, Water-to-air transfer of nano/microsized particulates: Enrichment effect in bubble bursting jet drops, Nano Lett. **13**, 5626 (2022).
[30] J. A. Quinn, R. A. Steinbrook, and J. L. Anderson, Breaking bubbles and the water-to-air transport of particulate matter, Chem. Eng. Sci. **30**, 1177 (1975).
[31] P. L. Walls, L. Henaux, and J. C. Bird, Jet drops from bursting bubbles: How gravity and viscosity couple to inhibit droplet production, Phys. Rev. E **92**, 4 (2015).
[32] Z. Dai, D. Fornasiero, and J. Ralston, Particle-bubble collision models—A review, Adv. Colloid Interface Sci. **85**, 231 (2000).
[33] T. Miettinen, J. Ralston, and D. Fornasiero, The limits of fine particle flotation, Miner. Eng. **23**, 420 (2010).
[34] See Supplemental Material at http://link.aps.org/supplemental/10.1103/PhysRevLett.130.054001 for further details about experiments and numerical simulations, as well as modeling assumptions and experimental validation of selective aerosolization. A video of the numerics with forward and backward Lagrangian particle tracking is also included, which includes Refs. [35–41].
[35] H. Schulze, *Flotation as Heterocoagulation Process: Possibilities of Calculating the Probability of Flotation, in Coagulation and Flocculation* (Dekker, Boca Raton, 1993), pp. 321–353.
[36] S. H. Park, C. Park, J. Y. Lee, and B. Lee, A simple parameterization for the rising velocity of bubbles in a liquid pool, Nucl. Eng. Technol. **49**, 692 (2017).
[37] D. Michael and P. Norey, Particle collision efficiencies for a sphere, J. Fluid Mech. **37**, 565 (1969).
[38] G. S. Dobby and J. A. Finch, A model of particle sliding time for flotation size bubbles, J. Colloid Interface Sci. **109**, 493 (1986).
[39] G. Dobby and J. Finch, Particle size dependence in flotation derived from a fundamental model of the capture process, Int. J. Miner. Process. **21**, 241 (1987).
[40] D. Vella, P. Aussillous, and L. Mahadevan, Elasticity of an interfacial particle raft, Europhys. Lett. **68**, 212 (2004).
[41] K. L. Sutherland, Physical chemistry of flotation. XI: Kinetics of the flotation process, J. Phys. Colloid Chem. **52**, 394 (1948).
[42] S. Popinet, The gerris flow solver (2021), https://gfs.sourceforge.net/wiki/index.php/Main_Page.
[43] S. Popinet, Gerris: A tree-based adaptive solver for the incompressible euler equations in complex geometries, J. Comput. Phys. **190**, 572 (2003).
[44] S. Popinet, An accurate adaptive solver for surface-tension-driven interfacial flows, J. Comput. Phys. **228**, 5838 (2009).
[45] L. Deike, E. Ghabache, G. Liger-Belair, A. K. Das, S. Zaleski, S. Popinet, and T. Séon, Dynamics of jets produced by bursting bubbles, Phys. Rev. Fluids **3**, 1 (2018).
[46] O. McRae, K. R. Mead, and J. C. Bird, Aerosol agitation: Quantifying the hydrodynamic stressors on particulates encapsulated in small droplets, Phys. Rev. Fluids **6**, L031601 (2021).